Spin-orbit coupling induced demagnetization in Ni: *Ab initio* nonadiabatic molecular dynamics perspective

Zhenfa Zheng, Qijing Zheng, and Jin Zhao

Phys. Rev. B **105**, 085142 — Published 24 February 2022

DOI: 10.1103/PhysRevB.105.085142

Spin-orbit Coupling Induced Demagnetization in Ni: A Perspective from *Ab Initio* Nonadiabatic Molecular Dynamics Investigation

Zhenfa Zheng,[1] Qijing Zheng,[1,*] and Jin Zhao[1,2,3,†]

[1] *ICQD/Hefei National Laboratory for Physical Sciences at Microscale, and CAS Key Laboratory of Strongly-Coupled Quantum Matter Physics, and Department of Physics, University of Science and Technology of China, Hefei, Anhui 230026, China*

[2] *Department of Physics and Astronomy, University of Pittsburgh, Pittsburgh, Pennsylvania 15260, USA*

[3] *Synergetic Innovation Center of Quantum Information & Quantum Physics, University of Science and Technology of China, Hefei, Anhui 230026, China*

(Dated: January 31, 2022)

Spin-orbit coupling (SOC), which can induce spin-flip during the relaxation of photoexcited charge carrier, plays a crucial role in spin dynamics. In this work, we have used time-domain *ab initio* nonadiabatic molecular dynamics (NAMD) method to study the SOC induced ultrafast demagnetization in Ni at 300 K. The spin-diabatic representation using spin-polarized Kohn-Sham (KS) basis sets and spin-adiabatic representation using spinor basis sets have been applied, and both of them achieve demagnetization in Ni with a timescale around 100 fs. The spin-diabatic representation suggests a picture that the electron-phonon coupling (EPC) provides direct energy relaxation channel among the same-spin states, while the SOC can induce spin-flip. After photoexcitation, it is found the spin-minority electrons relax to the same-spin states rather than the opposite-spin states, since EPC is larger than SOC by one order of magnitude. By contrast, for the spin-majority electrons, spin-flip occurs since there are no empty same-spin states as electron acceptor above the Fermi level. The different relaxation pathways for spin-majority and spin-minority electrons induce the demagnetization. The spin-adiabatic representation provides an Elliott-Yafet spin-phonon scattering picture. The SOC induced reduction of magnetic moment in Ni may induce magnon to drive further demagnetization. The *ab initio* NAMD simulation provides a critical angle to understand how the SOC and EPC affect demagnetization process in Ni.

I. INTRODUCTION

Understanding, predicting, and ultimately controlling excited carrier dynamics are at the heart of diverse physics, chemistry and material science, which has many applications in photovoltaics, photocatalysis, plasmonics, spintronics and valleytronics et al. After photoexcitation, the excited carriers have different relaxation pathways in which various mechanisms, including electron-phonon, electron-hole, electron-electron, spin-orbit interactions et al., come into play. To understand these complex excited carrier dynamics, real-time *ab initio* investigations are essential.

Generally, during the non-radiative relaxation, the energy of excited carriers is transferred to the phonon system by electron-phonon coupling (EPC). The recently developed *ab initio* nonadiabatic molecular dynamics (NAMD) approach[1], which combines time-dependent Kohn-Sham (TDKS) equation with surface hopping scheme and *ab initio* molecular dynamics, accounts for EPC in real-time domain. In recent decades, it has been applied successfully to many solid systems for the investigation of nonradiative relaxation[2, 3]. Very recently, GW+real-time BSE-NAMD method was developed, in which the electron-hole (e-h) interaction is considered based on GW+BSE[4]. Different from the EPC and e-h interaction, the spin-orbit coupling (SOC) provides another relaxation channel for the photoexcited charge carrier. Analogous to a magnetic field, SOC can induce spin-flip during the charge relaxation by transferring the spin angular momentum to the orbital angular momentum, which provides a unique way to change the magnetization in an ultrafast manner. In such a process, the spin can scatter with phonons where the SOC and the EPC collectively affect the excited carrier energy and spin relaxation. Therefore, SOC-included *ab initio* NAMD method is a powerful tool for the design of ultrafast spintronic materials and devices. In previous work, people have studied how the SOC affects the charge transfer or hot carrier relaxation by *ab initio* NAMD simulation[5, 6]. Yet, it has not been applied to study the SOC induced spin dynamics.

The ferromagnetic metal nickel provides an excellent prototypical system to study how the SOC and lattice phonon excitation affect the spin dynamics coherently. Ultrafast demagnetization induced by photoexcitation in Ni has been observed for decades[7]. Numerous experiments have been performed on Ni ferromagnets and ferrimagnetic alloys, showing that the magnetization is quenched within 100 to 500 fs[8–11] and different physical mechanisms have been proposed[7, 9, 12–26]. Among all these mechanisms, the spin-phonon scattering via SOC leading to spin-flip was proposed to play an important role. As early as 1990s', the phenomenological three-temperature model has been proposed, describing the interaction between the electron,

* zqj@ustc.edu.cn
† zhaojin@ustc.edu.cn

spin and lattice sub-systems.*[cite]* Later, Koopmans et al. introduced a microscopic model based on the Elliott-Yafet type of spin-phonon scattering, which is described using a spin-flip probability determined by the SOC-induced spin-mixing[14]. Oppeneer et al. introduced the full electron-phonon matrix elements and phonon dispersions obtained by *ab initio* calculations to simulate such Elliott-Yafet spin-phonon scattering[16]. All these previous works provide valuable insights into the spin-phonon scattering induced spin-flip, in which the electron, spin and lattice systems interact with each other through EPC and SOC. However, here we propose that a real-time *ab initio* study including the electron, lattice and spin degrees of freedom is essential for a complementary physical picture at the atomic scale.

In this work, the time-dependent *ab initio* NAMD simulations are performed with spin-diabatic and spin-adiabatic representations, respectively. In the spin-diabatic picture, after photoexcitation, on one hand, the EPC provides a direct energy relaxation channel among the same-spin electronic states, through which the energy will be transferred from the photoexcited electrons to the lattice without changing the spin. On the other hand, SOC provides spin-flip channel between the opposite-spin electronic states. Via this channel, in addition to the energy relaxation, there will also be the angular momentum transfer from the spin to the orbital mediated by SOC. Such two different relaxation channels compete with each other. We find that in bulk Ni, because the EPC is larger than SOC, photo-excited spin minority electrons prefer to relax through the EPC channel to the same-spin states, rather than flip their spins through the SOC. However, for the photo-excited spin majority electrons, there are no unoccupied same-spin states above the Fermi level (E_f) as electron acceptor, and in that case the spin-flip occurs with a timescale around 100 fs. Such different dynamical behaviors result in the decrease of spin majority electrons and the increase of spin minority electrons, which lead to initiatory magnetic loss and will induce magnon to drive further demagnetization. The spin-adiabatic representation gives similar demagnetization timescale. In this representation the spin-up and spin-down orbitals are mixed due to SOC, forming spinor basis sets, and the spin relaxation process can be understood as an Elliott-Yafet-like process. Our study provides a clear picture that SOC can induce demagnetization of Ni at the atomic scale. In addition, it reveals that the spin majority and spin minority electrons have different lifetime as their relaxations are driven by SOC and EPC respectively. It will lead to different mean free path [27], which is the dominant reason of super diffusive spin transfer [9, 25]. This work also paves a way for the application of time-dependent *ab initio* NAMD simulation for the photoexcited spin dynamics, which is important for the understanding and design of photo-controlled ultrafast spintronic devices.

II. METHOD

In this article, the spin dynamics is simulated using home-made code Hefei-NAMD. This program is based on the framework of fewest-switches surface hopping (FSSH)[28] combined with time-dependent density function theory (TDDFT) [1, 29, 30], which has been used in numerous studies of condensed materials[2, 31–41]. The nuclear degrees of freedom are treated classically and are unaffected by the dynamics of the electronic degrees of freedom, which is known as classical-path approximation (CPA) [1]. The electronic Hamiltonian depends parametrically on the classical nuclear variables, which evolves along an *ab initio* molecular dynamics (AIMD) trajectory. Then the time-dependent Schrödinger equation (TDSE) of electronic state including SOC can be written as:

$$i\hbar\frac{\partial}{\partial t}\left|\Phi(\mathbf{r},\mathbf{R},\sigma)\right\rangle = \hat{\mathcal{H}}(\mathbf{r},\mathbf{R},\sigma)\left|\Phi(\mathbf{r},\mathbf{R},\sigma)\right\rangle \tag{1}$$

where σ is the index for spin and the total Hamiltonian is given by a spin-free and an SOC term

$$\hat{\mathcal{H}}^{\mathrm{tot}}(\mathbf{r},\mathbf{R},\sigma) = \hat{\mathcal{H}}_0(\mathbf{r},\mathbf{R}(t)) + \hat{\mathcal{H}}^{\mathrm{soc}}(\mathbf{r},\mathbf{R}(t)) \tag{2}$$

The wavefuntion can be expanded using Kohn-Sham (KS) orbitals $\{|\psi_i(\mathbf{r};\mathbf{R}(t))\rangle\}$ as basis sets,

$$\left|\Phi(\mathbf{r},\mathbf{R},\sigma)\right\rangle = \sum_i \left|\psi_i\right\rangle\left\langle\psi_i|\Phi(\mathbf{r},\mathbf{R},\sigma)\right\rangle = \sum_i c_i\left|\psi_i\right\rangle \tag{3}$$

And substituting Eq. (3) into Eq. (1), we can get the equation for the expanding coefficients

$$\begin{aligned} i\hbar\frac{\partial c_i(t)}{\partial t} &= \sum_j \left[\left\langle\psi_i|\hat{\mathcal{H}}^{\mathrm{tot}}|\psi_j\right\rangle - i\hbar\left\langle\psi_i|\frac{\mathrm{d}}{\mathrm{d}t}|\psi_j\right\rangle\right] c_j(t) \\ &= \sum_j \left[\left\langle\psi_i|\hat{\mathcal{H}}_0|\psi_j\right\rangle + \left\langle\psi_i|\hat{\mathcal{H}}^{\mathrm{soc}}|\psi_j\right\rangle - i\hbar\left\langle\psi_i|\frac{\mathrm{d}}{\mathrm{d}t}|\psi_j\right\rangle\right] c_j(t) \\ &= \sum_j \left[H^0_{ij} + H^{\mathrm{soc}}_{ij} - i\hbar T_{ij}\right] c_j(t) \end{aligned} \tag{4}$$

where $T_{ij} = \langle\psi_i|\frac{\mathrm{d}}{\mathrm{d}t}|\psi_j\rangle$ can be transformed to $\dot{\mathbf{R}}\cdot(\varepsilon_j - \varepsilon_i)^{-1}\cdot\langle\psi_i|\nabla_{\mathbf{R}}\hat{\mathcal{H}}_0|\psi_j\rangle$ and this term is contributed by EPC. For the *ab initio* NAMD without SOC, this term

is the nonadiabatic coupling (NAC), which determines the hopping probability between different KS orbitals. Here, besides the EPC contribution, the contribution of SOC is also added into NAC. The spin-orbit Hamiltonian is given by

$$\hat{\mathcal{H}}^{\mathrm{soc}} = \frac{\hbar\sigma \cdot \mathbf{p} \times \nabla v_{KS}(\mathbf{r})}{4m^2c^2}, \tag{5}$$

$v_{KS}(\mathbf{r})$ is the spin-independent part of the Kohn-Sham potential. Due to the derivative of the Kohn-Sham potential in Eq. (5), the spin-orbit coupling is dominated by the regions close to the nuclei. In the PAW formalism, the all-electron orbitals in these regions can be expanded as

$$\psi_i = \sum_k \langle \tilde{p}_k | \tilde{\psi}_i \rangle \, |\phi_k\rangle \tag{6}$$

where $|\tilde{p}_k\rangle$ and $\left|\tilde{\phi}_k\right\rangle$ are the projector function and all-electron partial waves, respectively. The SOC matrix elements then become

$$H_{ij}^{\mathrm{soc}} = \sum_{kl} \langle \tilde{\psi}_i | \tilde{p}_k \rangle \, \langle \phi_k | \hat{\mathcal{H}}^{\mathrm{soc}} | \phi_l \rangle \, \langle \tilde{p}_l | \tilde{\psi}_j \rangle \tag{7}$$

In our simulations, the matrix elements in the right-hand-side of Eq.(7) are calculated by VASP.

In the NAMD simulation, two types of basis set are used in Eq. (3). One is the spin-polarized KS orbitals, which are themselves eigenfunctions of $\hat{\mathcal{H}}_0$ and shall be referred to as the spin-diabatic representation. In this case, the matrix elements not only include the EPC term (T_{ij}) but also the SOC term (H_{ij}^{soc}). While the nonradiative relaxation between the states with same-spin is determined by T_{ij}, the spin-flip probability is decided by SOC. These two different contributions can be distinguished clearly. On the other hand, we can also diagonalize the Hamiltonian in Eq. (4) to get the spinor basis sets for the time propagation, which is referred to as the spin-adiabatic representation. The two-component spinor wavefunction can be written as:

$$|\psi_i\rangle = \begin{pmatrix} |\psi_i^{\uparrow}\rangle \\ |\psi_i^{\downarrow}\rangle \end{pmatrix} \tag{8}$$

In this case, the NAC between different spinor states can be expressed as

$$T_{ij} = \langle \psi_i | \frac{\mathrm{d}}{\mathrm{d}t} | \psi_j \rangle = \left(\langle \psi_i^{\uparrow}|, \langle \psi_i^{\downarrow}| \right) \frac{\mathrm{d}}{\mathrm{d}t} \begin{pmatrix} |\psi_i^{\uparrow}\rangle \\ |\psi_i^{\downarrow}\rangle \end{pmatrix} \tag{9}$$

In the spin-adiabatic representation, both the EPC and SOC effects are mixed together in the NAC elements. The spin-diabatic and spin-adiabatic representations have been introduced and discussed in previous reference[42].

The AIMD trajectory and spin-polarized KS basis sets are calculated by Vienna *ab initio* Simulation Package (VASP)[43, 44]. The electron-nuclei interaction is described by the projector augmented wave (PAW) method[45]. For the exchange-correlation functional we use the generalized gradient approximation of Perdew-Burke-Ernzerhof (GGA-PBE)[46]. Structures are fully relaxed until residual forces on constituent atoms become smaller than 0.01 eV/Å, and total electronic energies are converged to 10^{-5} eV. An energy cut-off of 450 eV and a Monkhorst-Pack k-point sampling grid of $15 \times 15 \times 15$ for unit cell and $3 \times 3 \times 3$ for supercell are sufficient for convergence.

The electronic structure is calculated using the optimized unit cell at 0 K. For the molecular dynamics simulations, in order to sample enough states of different k-points, we use a $2 \times 2 \times 2$ conventional face-centered cubic (fcc) supercell, which involves 32 Ni atoms. After the geometry optimization, we use velocity-rescaling to bring the temperature of the system to 300 K. A 5 ps *ab initio* molecular dynamics trajectory is then generated with a time step of 1 fs. The NAMD results are obtained by averaging over 100 different initial configurations chosen randomly from the first 3 ps of the molecular dynamics trajectory. For each chosen structure, we sample 20000 NAMD trajectories with 1 ps in length for each one.

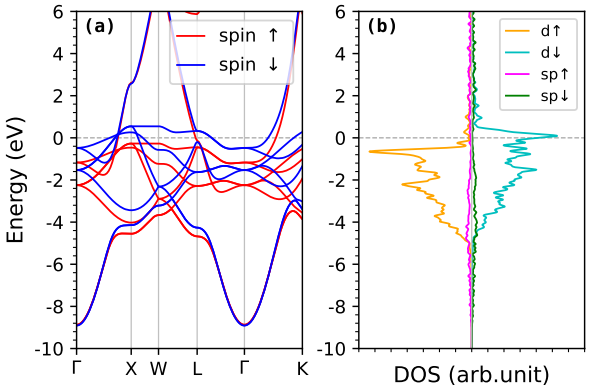

FIG. 1. Band structure (a), *sp*- and *d*-projected density of state (b) for Ni. The Fermi level is chosen as energy zero.

III. RESULTS AND DISSCUSSION

Before we discuss the *ab initio* NAMD results, it is instructive to study the electronic structure of Ni. Its ground state is ferromagnetic, where the magnetic moment originates from the band split of 3*d* orbitals. Fig. 1 shows the band structure and density of states (DOS) of Ni. In the energy range from −5 to 0.5 eV, the bands are mainly contributed by *d* orbitals and the split of *d* bands is about 0.8 eV. Due to the split of *d* bands, spin-up states are totally occupied while some spin-down states are unoccupied. Thus, we can define the spin-up and spin-down electrons as spin majority and minority, respectively. Comparing to *s* and *p* (*sp*) orbitals, the *d* orbitals are more localized in real space, which leads

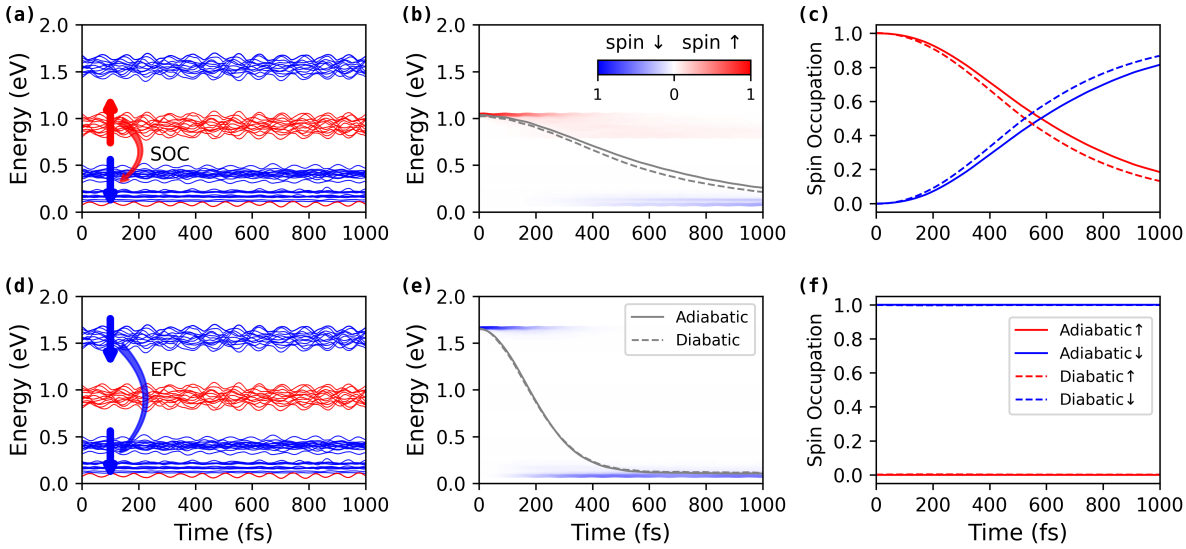

FIG. 2. Spin dynamics of spin majority (a-c) and spin minority (d-f) in NAMD simulations. (a, d) Energy evolution of the electron states at Γ point in the reciprocal space of Ni supercell. (b, e) Energy relaxation of excited electron, where the color map shows the orbital localization. (c, f) Spin relaxation of excited electron. In panel (b), (c), (e) and (f), solid and dashed lines are results from spin-adiabatic and spin-diabatic representations, respectively.

to weaker dispersion in reciprocal space. Therefore, as shown in Fig. 1(b), the DOS of d bands are higher than sp bands. The DOS of the $2 \times 2 \times 2$ orthogonal supercell reproduce the major characters of the electronic structure (See Supplemental Materials [47]). These features of Ni electronic structure play important roles in the spin dynamics that will be discussed below.

We then study the dynamics of photoexcited electrons with different spins. Fig. 2(a) and (d) show the time evolution of KS eigenstates at Γ point in the reciprocal space of Ni supercell, in which the spin-up and spin-down states are shown by red and blue lines, respectively. The initial and final states of the electron relaxation are marked by arrows. The initial states are the sp orbital at 1.0 and 1.5 eV for spin-up and spin-down electrons, respectively. And the final states are the spin-down d orbital close to the E_f. Fig. 2(b, c) and (e, f) show the time-dependent energy and spin relaxation of the photoexcited electron by diabatic and adiabatic representations. Fig. 2(b, c) describes the dynamics of a spin-up electron, which is initially excited at 1.0 eV above the E_f. It is found this spin-up electron decays to spin-down unoccupied states around E_f with a time scale of 567 fs [Fig. 2(b)], which is fitted by using an gaussian function. Such relaxation process accompanies with spin-flip from majority to minority [Fig. 2(c)], which will reduce the magnetic moments of Ni. By contrast, the photoexcited spin-down electron shows different dynamical behavior. As shown in Fig. 2(e, f), when the spin-down electron is excited at 1.5 eV above E_f. It will relax to the spin-down unoccupied states at E_f with a timescale of 242 fs [Fig. 2(e)]. During this process, no spin-flip occurs[Fig. 2(f)]. The spin-down electron will directly transfer its energy to the lattice through EPC and tends to conserve its spin. It can be noted that spin-diabatic and spin-adiabatic representations provide very similar dynamical behavior.

In the spin-diabatic representation, we can directly compare the EPC between the same-spin states with the SOC, as shown in Fig. 3. It is noted that EPC elements between same-spin states are larger than SOC between opposite-spin states by an order of magnitude. It explains why the spin-down electron prefers to relax to the lower spin-down states via EPC, rather than to the spin-up states through SOC. For the spin-up electron, however, because there are no spin-up unoccupied states above E_f, spin-flip through SOC is the only relaxation channel. SOC also exists for the same-spin electronic states. It can be seen that the SOC depends on the orbital composition. Comparing the d-d, d-sp and sp-sp SOC, one can find that d-d SOC is the largest while sp-sp SOC is the smallest. When the spin-down electron is excited to sp band above E_f, because SOC of d-sp is larger than that of sp-sp, SOC also stimulates the relaxation of spin-down electron to the spin-down d bands close to Fermi level, rather than to the spin-up sp bands. We note that the DFT calculations may overestimate the exchange splitting [48]. However, we propose such overestimation will not affect the existence of two different electron relaxation channels, although the magnitudes of EPC and SOC may be affected slightly. High-level calculations are necessary to revisit this problem in the future.

Under the spin-adiabatic representation, the spinor basis is a mixture of spin-up and spin-down states. SOC determines the magnitude of spin-mixing and the spin

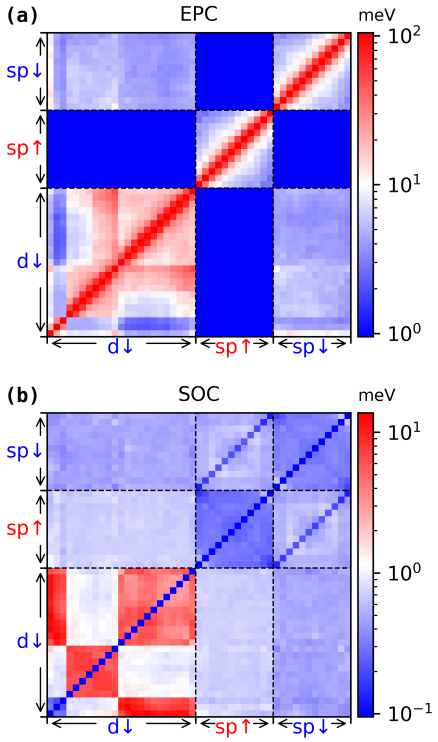

FIG. 3. EPC (a) and SOC (b) between electronic states in order of energy as shown in Fig. 2(a, d). "$d\downarrow$" denotes spin-down states at 0–0.5 eV, which are mainly contributed by d orbitals; "$sp\uparrow$" and "$sp\downarrow$" denote spin-up and spin-down states around 1.0 and 1.5 eV respectively, which are mainly contributed by sp orbitals.

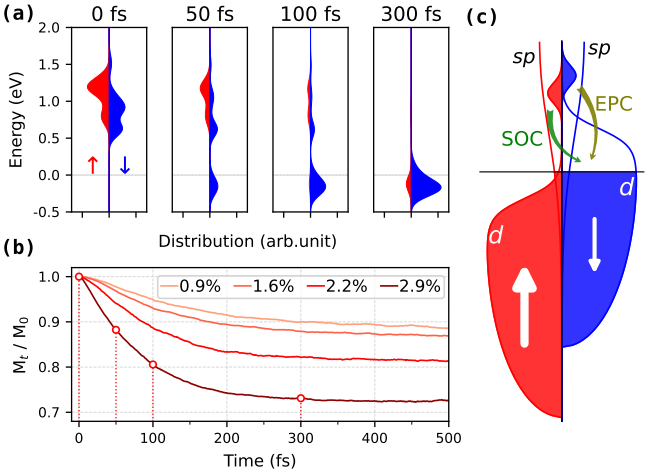

FIG. 4. (a) Distribution of electrons at different snapshots by performing multi-electrons NAMD simulation. (b) Evolution of relative magnetic moments at different electron excitation rates. (c) The schematic mechanism of SOC-induced demagnetization in Ni.

relaxation process can be understood as an Elliott-Yafet-like spinor-phonon scattering process[13, 16], in which the spin relaxation is accompanied with a phonon emission. The results shown in Fig. 2 are based on single electron excitation. To further confirm the SOC induced demagnetization picture, we investigate the multi-electron dynamics using spin-adiabatic representation. To sample major character of the electronic structure, the multi-electron NAMD simulations are performed at different irreducible k-points in the $3 \times 3 \times 3$ k-grid and subsequently summed the results with corresponding k-point weights (See Supplemental Materials [47]). In multi-electron simulations, same number of spin-up and spin-down electrons are excited initially to the states at 0.5–1.5 eV above the E_f. Fig. 4(a) shows the snapshots of DOS contributed by excited electrons of two spin components at different times with 2.9% electrons excited. It can be seen some of the spin-up electrons flip their spins during the relaxation. Therefore, as shown in Fig. 4(b), the relative magnetic moment M_t/M_0 decrease from 1.0 to 0.89 within the first 50 fs, then reaches 0.81 at 100 fs and further converges to 0.73 at 300 fs, where M_0 and M_t are the initial and time-dependent magnetic moments at time t, respectively. We have further investigated the influence of photo excitation rate on the demagnization magnitude. As shown in Fig. 4(b), the results with 2.2%, 1.6% and 0.9% photoexcitation rates suggest the demagnization magnitude decreases along with the decreasing of excitation rate. The time scales of demagnetization obtained by fitting with an exponential decay functions are 142, 122, 95 and 75 fs for electron excitation rates of 0.9%, 1.6%, 2.2% and 2.9%, respectively, suggesting a faster demagnization with higher photoexciation rate. In multi-electron simulations, some spin-up electrons are initially photoexcited to the d orbitals which are lower than the sp orbitals. Therefore, some spin-flip events occur between d orbitals, which have stronger SOC, leading to a faster demagnetization comparing to the single-electron excitation.

The results shown in Fig. 2 and Fig. 4 also suggest that the spin majority electrons has longer lifetime than the spin minority electrons. This is because the decay rate of spin majority and spin minority electrons is determined by the SOC and EPC respectively, and EPC is one order of magnitude larger than SOC. The longer lifetime of spin majority electrons may lead to larger mean free path the super-diffusive spin transport and result in further demagnetization as reported by ref.[25, 27]

In this work, we show that spin-diabatic and spin-adiabatic representations give very similar timescales for spin flipping. We should point out that in the spin-diabatic representation, the SOC is treated as a perturbation and it can provide reasonable results only when SOC is small [42, 49]. By contrast, the spin-adiabatic approach is more applicable. Yet in the spin-diabatic representation, the contribution by SOC and EPC can be clearly distinguished and it is useful to understand the physical picture of spin dynamics. In this study we explicitly consider the role of SOC and EPC in the spin relaxation in Ni at the *ab initio* level. Yet, it can be

seen that the demagnetization magnitude predicted by the multi-electron simulation is weaker than the experimental value[7]. We recognize that the effects of photoexcitation, electron-electron scattering as well as the magnon formation and dynamics are not included in the simulation. These effects can further enhance the demagnetization in Ni [17–19, 22, 26, 50]. For example, Töws and Pastor proposed that the interplay between the electron-electron interaction and SOC induces the ultrafast demagnetizaiton [26]. Additionally, the demagnetization is related to electron excitation rate, and electron excitation rates are proportional to laser fluence (See Supplemental Materials [47]). A larger laser fluence will induce more demagnetization, which have bee confirmed in many works[10, 12, 14, 17, 21].

IV. CONCLUSION

To conclude, we have used SOC included *ab initio* NAMD simulation to investigate the spin dynamics in Ni. The spin-diabatic and spin-adiabatic representations have been used. The physical picture provided by the spin-diabatic representation is schematically shown in Fig. 4(c), in which the EPC and SOC provide the direct energy relaxation channel between the same-spin states and the spin splitting channel between opposite-spin states, respectively. For the photoexcited spin-minority (spin-down) electron, since EPC is larger than SOC, it prefers to relax to the same-spin states without spin-flip. Yet for the photoexcited spin-majority (spin-up) electron, there are no the same-spin unoccupied states above E_f, therefore, the spin-flip occurs, which can induce demagnetization. The adiabatic presentation provides an Elliott-Yafet-like spinor-phonon scattering picture. Both representations give similar demagnetization timescale. The spin-majority electron has a longer lifetime than the spin-minority electron, which explains the super-diffusive spin transfer. The simulation of multi-electron relaxation shows such SOC induced demagnetization has a time scale around 100 fs, which is in agreement with previous experimental results. Our study provides unique insight into the mechanism of demagnetization in Ni, it also paves a way for the wide applications of SOC included *ab initio* NAMD simulation in spin dynamics research field.

ACKNOWLEDGMENTS

J.Z. acknowledges the support of the National Key Foundation of China, Department of Science and Technology, grant no. 2017YFA0204904; The National Natural Science Foundation of China (NSFC), grant nos. 11620101003, 11974322. Calculations were performed, in part, at the Environmental Molecular Sciences Laboratory at the PNNL, a user facility sponsored by the DOE Office of Biological and Environmental Research, and Supercomputing Center at USTC.

[1] C. F. Craig, W. R. Duncan, and O. V. Prezhdo, Trajectory surface hopping in the time-dependent Kohn-Sham approach for electron-nuclear dynamics, Phys. Rev. Lett. **95**, 163001 (2005).
[2] Q. Zheng, W. Chu, C. Zhao, L. Zhang, H. Guo, Y. Wang, X. Jiang, and J. Zhao, Ab initio nonadiabatic molecular dynamics investigations on the excited carriers in condensed matter systems, WIREs Comput Mol Sci **9**, e1411 (2019).
[3] R. Long, O. V. Prezhdo, and W. Fang, Nonadiabatic charge dynamics in novel solar cell materials, WIREs Comput Mol Sci **7**, e1305 (2017).
[4] X. Jiang, Q. Zheng, Z. Lan, W. A. Saidi, X. Ren, and J. Zhao, Real-time GW-BSE investigations on spin-valley exciton dynamics in monolayer transition metal dichalcogenide, Sci. Adv. **7**, eabf3759 (2021).
[5] W. Li, L. Zhou, O. V. Prezhdo, and A. V. Akimov, Spin-orbit interactions greatly accelerate nonradiative dynamics in lead halide perovskites, ACS Energy Lett. **3**, 2159 (2018).
[6] X.-Y. Liu, J.-J. Yang, W.-K. Chen, A. V. Akimov, W.-H. Fang, and G. Cui, Spin-orbit coupling accelerates the photoinduced interfacial electron transfer in a fullerene-based perovskite heterojunction, J. Phys. Chem. Lett. **12**, 1131 (2021).
[7] E. Beaurepaire, J.-C. Merle, A. Daunois, and J.-Y. Bigot, Ultrafast spin dynamics in ferromagnetic nickel, Phys. Rev. Lett. **76**, 4250 (1996).
[8] C. Stamm, T. Kachel, N. Pontius, R. Mitzner, T. Quast, K. Holldack, S. Khan, C. Lupulescu, E. F. Aziz, M. Wietstruk, H. A. Dürr, and W. Eberhardt, Femtosecond modification of electron localization and transfer of angular momentum in nickel, Nature Mater **6**, 740 (2007).
[9] D. Rudolf, C. La-O-Vorakiat, M. Battiato, R. Adam, J. M. Shaw, E. Turgut, P. Maldonado, S. Mathias, P. Grychtol, H. T. Nembach, T. J. Silva, M. Aeschlimann, H. C. Kapteyn, M. M. Murnane, C. M. Schneider, and P. M. Oppeneer, Ultrafast magnetization enhancement in metallic multilayers driven by superdiffusive spin current, Nat Commun **3**, 1037 (2012).
[10] P. Tengdin, W. You, C. Chen, X. Shi, D. Zusin, Y. Zhang, C. Gentry, A. Blonsky, M. Keller, P. M. Oppeneer, H. C. Kapteyn, Z. Tao, and M. M. Murnane, Critical behavior within 20 fs drives the out-of-equilibrium laser-induced magnetic phase transition in nickel, Sci. Adv. **4**, eaap9744 (2018).
[11] M. Hennecke, I. Radu, R. Abrudan, T. Kachel, K. Holldack, R. Mitzner, A. Tsukamoto, and S. Eisebitt, Angular momentum flow during ultrafast demagnetization of a ferrimagnet, Phys. Rev. Lett. **122**, 157202 (2019).
[12] J. Hohlfeld, E. Matthias, R. Knorren, and K. H. Bennemann, Nonequilibrium magnetization dynamics of nickel, Phys. Rev. Lett. **78**, 4861 (1997).
[13] B. Koopmans, J. J. M. Ruigrok, F. D. Longa, and W. J. M. de Jonge, Unifying ultrafast magnetization dynamics, Phys. Rev. Lett. **95**, 267207 (2005).

[14] B. Koopmans, G. Malinowski, F. Dalla Longa, D. Steiauf, M. Fähnle, T. Roth, M. Cinchetti, and M. Aeschlimann, Explaining the paradoxical diversity of ultrafast laser-induced demagnetization, Nature Mater **9**, 259 (2009).

[15] M. Fähnle, J. Seib, and C. Illg, Relating Gilbert damping and ultrafast laser-induced demagnetization, Phys. Rev. B **82**, 144405 (2010).

[16] K. Carva, M. Battiato, and P. M. Oppeneer, Ab initio investigation of the Elliott-Yafet electron-phonon mechanism in laser-induced ultrafast demagnetization, Phys. Rev. Lett. **107**, 207201 (2011).

[17] E. Carpene, E. Mancini, C. Dallera, M. Brenna, E. Puppin, and S. De Silvestri, Dynamics of electron-magnon interaction and ultrafast demagnetization in thin iron films, Phys. Rev. B **78**, 174422 (2008).

[18] A. B. Schmidt, M. Pickel, M. Donath, P. Buczek, A. Ernst, V. P. Zhukov, P. M. Echenique, L. M. Sandratskii, E. V. Chulkov, and M. Weinelt, Ultrafast magnon generation in an Fe film on cu(100), Phys. Rev. Lett. **105**, 197401 (2010).

[19] M. Krauß, T. Roth, S. Alebrand, D. Steil, M. Cinchetti, M. Aeschlimann, and H. C. Schneider, Ultrafast demagnetization of ferromagnetic transition metals: The role of the coulomb interaction, Phys. Rev. B **80**, 180407 (2009).

[20] D. Steil, S. Alebrand, T. Roth, M. Krauß, T. Kubota, M. Oogane, Y. Ando, H. C. Schneider, M. Aeschlimann, and M. Cinchetti, Band-structure-dependent demagnetization in the heusler alloy $Co_2Mn_{1-x}Fe_xSi$, Phys. Rev. Lett. **105**, 217202 (2010).

[21] G. P. Zhang and W. Hübner, Laser-induced ultrafast demagnetization in ferromagnetic metals, Phys. Rev. Lett. **85**, 3025 (2000).

[22] Z. Chen and L.-W. Wang, Role of initial magnetic disorder: A time-dependent ab initio study of ultrafast demagnetization mechanisms, Sci. Adv. **5**, eaau8000 (2019).

[23] S. R. Acharya, V. Turkowski, G. P. Zhang, and T. S. Rahman, Ultrafast electron correlations and memory effects at work: Femtosecond demagnetization in Ni, Phys. Rev. Lett. **125**, 017202 (2020).

[24] G. P. Zhang, W. Hübner, G. Lefkidis, Y. Bai, and T. F. George, Paradigm of the time-resolved magneto-optical Kerr effect for femtosecond magnetism, Nature Phys **5**, 499 (2009).

[25] M. Battiato, K. Carva, and P. M. Oppeneer, Superdiffusive spin transport as a mechanism of ultrafast demagnetization, Phys. Rev. Lett. **105**, 027203 (2010).

[26] W. Töws and G. M. Pastor, Many-body theory of ultrafast demagnetization and angular momentum transfer in ferromagnetic transition metals, Phys. Rev. Lett. **115**, 217204 (2015).

[27] V. P. Zhukov, E. V. Chulkov, and P. M. Echenique, Lifetimes and inelastic mean free path of low-energy excited electrons in Fe, Ni, Pt, and Au: Ab initio GW+T calculations, Phys. Rev. B **73**, 125105 (2006).

[28] J. C. Tully, Molecular dynamics with electronic transitions, J. Chem. Phys. **93**, 1061 (1990).

[29] A. V. Akimov and O. V. Prezhdo, The PYXAID program for non-adiabatic molecular dynamics in condensed matter systems, J. Chem. Theory Comput. **9**, 4959 (2013).

[30] A. V. Akimov and O. V. Prezhdo, Advanced capabilities of the PYXAID program: Integration schemes, decoherence effects, multiexcitonic states, and field-matter interaction, J. Chem. Theory Comput. **10**, 789 (2014).

[31] W. Chu, W. A. Saidi, Q. Zheng, Y. Xie, Z. Lan, O. V. Prezhdo, H. Petek, and J. Zhao, Ultrafast dynamics of photongenerated holes at a CH_3OH/TiO_2 rutile interface, J. Am. Chem. Soc. **138**, 13740 (2016).

[32] Q. Zheng, W. A. Saidi, Y. Xie, Z. Lan, O. V. Prezhdo, H. Petek, and J. Zhao, Phonon-assisted ultrafast charge transfer at van der Waals heterostructure interface, Nano Lett. **17**, 6435 (2017).

[33] C. Zhao, Q. Zheng, J. Wu, and J. Zhao, Ab initio nonadiabatic molecular dynamics investigation on the dynamics of photogenerated spin hole current in Cu-doped MoS_2, Phys. Rev. B **96**, 134308 (2017).

[34] L. Zhang, Q. Zheng, Y. Xie, Z. Lan, O. V. Prezhdo, W. A. Saidi, and J. Zhao, Delocalized impurity phonon induced Electron–Hole recombination in doped semiconductors, Nano Lett. **18**, 1592 (2018).

[35] Y. Wang, H. Guo, Q. Zheng, W. A. Saidi, and J. Zhao, Tuning solvated electrons by polar-nonpolar oxide heterostructure, J. Phys. Chem. Lett. **9**, 3049 (2018).

[36] L. Zhang, W. Chu, Q. Zheng, A. V. Benderskii, O. V. Prezhdo, and J. Zhao, Suppression of electron-hole recombination by intrinsic defects in 2D monoelemental material, J. Phys. Chem. Lett. **10**, 6151 (2019).

[37] W. Chu, Q. Zheng, O. V. Prezhdo, and J. Zhao, CO_2 photoreduction on metal oxide surface is driven by transient capture of hot electrons: Ab initio quantum dynamics simulation, J. Am. Chem. Soc. **142**, 3214 (2020).

[38] W. Chu, Q. Zheng, O. V. Prezhdo, J. Zhao, and W. A. Saidi, Low-frequency lattice phonons in halide perovskites explain high defect tolerance toward electron-hole recombination, Sci. Adv. **6**, eaaw7453 (2020).

[39] Y. Tian, Q. Zheng, and J. Zhao, Tensile strain-controlled photogenerated carrier dynamics at the van der Waals heterostructure interface, J. Phys. Chem. Lett. **11**, 586 (2020).

[40] H. Guo, W. Chu, Q. Zheng, and J. Zhao, Tuning the carrier lifetime in black phosphorene through family atom doping, J. Phys. Chem. Lett. **11**, 4662 (2020).

[41] L. Zhang, W. Chu, C. Zhao, Q. Zheng, O. V. Prezhdo, and J. Zhao, Dynamics of photoexcited small polarons in transition-metal oxides, J. Phys. Chem. Lett. **12**, 2191 (2021).

[42] G. Granucci, M. Persico, and G. Spighi, Surface hopping trajectory simulations with spin-orbit and dynamical couplings, The Journal of Chemical Physics **137**, 22A501 (2012).

[43] G. Kresse and J. Hafner, Ab initio molecular dynamics for open-shell transition metals, Phys. Rev. B **48**, 13115 (1993).

[44] G. Kresse and J. Hafner, Ab initio molecular-dynamics simulation of the liquid-metal–amorphous-semiconductor transition in germanium, Phys. Rev. B **49**, 14251 (1994).

[45] P. E. Blöchl, Projector augmented-wave method, Phys. Rev. B **50**, 17953 (1994).

[46] J. P. Perdew, K. Burke, and M. Ernzerhof, Generalized gradient approximation made simple, Phys. Rev. Lett. **77**, 3865 (1996).

[47] See Supplemental Material at [URL] for DOS of supercell, multi-electron NAMD simulations at irreducible k-points and relationship between electron excitation rate and laser pump fluence, which includes Refs. [10,51].

[48] E. Şaşıoğlu, A. Schindlmayr, C. Friedrich, F. Freimuth, and S. Blügel, Wannier-function approach to spin excitations in solids, Phys. Rev. B **81**, 054434 (2010).

[49] T. Olsen, Designing in-plane heterostructures of quantum spin hall insulators from first principles: 1T'-MoS_2 with adsorbates, Phys. Rev. B **94**, 235106 (2016).

[50] J. Bigot and M. Vomir, Ultrafast magnetization dynamics of nanostructures, Annalen der Physik **525**, 2 (2013).

[51] T. Genieys, M. N. Petrakakis, G. D. Tsibidis, M. Sentis, and O. Utéza, Unravelling ultrashort laser excitation of nickel at 800 nm wavelength, Journal of Physics D: Applied Physics **54**, 495302 (2021).